REPORT DOCUMENTATION PAGE

Form Approved OMB No. 0704-0188

1. REPORT DATE *(DD-MM-YYYY)*	2. REPORT TYPE	3. DATES COVERED *(From - To)*
	Technical Papers	

4. TITLE AND SUBTITLE

5a. CONTRACT NUMBER

5b. GRANT NUMBER

5c. PROGRAM ELEMENT NUMBER

6. AUTHOR(S)

5d. PROJECT NUMBER
2302

5e. TASK NUMBER
M1G2

5f. WORK UNIT NUMBER

7. PERFORMING ORGANIZATION NAME(S) AND ADDRESS(ES)

Air Force Research Laboratory (AFMC)
AFRL/PRS
5 Pollux Drive
Edwards AFB CA 93524-7048

8. PERFORMING ORGANIZATION REPORT

9. SPONSORING / MONITORING AGENCY NAME(S) AND ADDRESS(ES)

Air Force Research Laboratory (AFMC)
AFRL/PRS
5 Pollux Drive
Edwards AFB CA 93524-7048

10. SPONSOR/MONITOR'S ACRONYM(S)

11. SPONSOR/MONITOR'S NUMBER(S)

12. DISTRIBUTION / AVAILABILITY STATEMENT

Approved for public release; distribution unlimited.

13. SUPPLEMENTARY NOTES

14. ABSTRACT

15. SUBJECT TERMS

16. SECURITY CLASSIFICATION OF:			17. LIMITATION OF ABSTRACT	18. NUMBER OF PAGES	19a. NAME OF RESPONSIBLE PERSON
a. REPORT	b. ABSTRACT	c. THIS PAGE			Leilani Richardson
Unclassified	Unclassified	Unclassified	A		19b. TELEPHONE NUMBER *(include area code)* (661) 275-5015

3k separate items are enclosed

fyi 6111

MEMORANDUM FOR IN-HOUSE PUBLICATIONS

FROM: PROI (TI) (STINFO)

14 Apr 98

SUBJECT: Authorization for Release of Technical Information, Control Number: AFRL-PR-ED-TP-1998-072
C.T. Liu "Monitoring Damage Initiation and Evolution in Filled Polymeric Materials Using Nondestructive Testing Techniques" ***NATO Sponsored Workshop*** **(Statement A)**

Monitoring Damage Initiation and Evolution in Filled Polymeric Materials Using Nondestructive Testing Techniques

C.T. Liu
Air Force Research Laboratory (AFMC)
10 East Saturn Boulevard
Edwards AFB CA 93524-7680

Abstract

This paper reviews the efforts expanded in evaluation of damage characteristics in highly filled polymeric materials under various loading conditions. Several different nondestructive testing techniques, including ultrasonic, acoustic imaging, and real-time radiography, have been used to monitor damage initiation and evolution processes. The nondestructive testing data were analyzed and the results are discussed.

Introduction

It is well known that, on the microscopic scale, a highly filled polymeric material can be considered a nonhomogeneous material. When this material is strained, depending on the magnitude of local stress and local strength, damage may be developed in the material. The damage developed in the material may be in the form of microvoids or microcracks in the binder or in the form of dewetting between the binder and the filler particle. The developed damage will not be confined to a specific location, rather it will diffuse into a relatively large area or zone. The growth of the damage in the material may occur by material tearing or by successive nucleation and coalescence of the microvoids.

Throughout the loading history, the progressive development and interaction of various damage modes change the state of the material and the response of the structures. In addition to the microdamage, large cracks can also develop in the material either during the manufacturing processes or by service loads. Therefore, to effectively use the material in structural applications one needs to understand the damage initiation and evolution processes, the effects of damage and crack development on the material's response, and the remaining strength and life of the structures.

Reliable performance of a structure in critical applications depends on assuring that the structure in service satisfies the conditions assumed in design and life prediction analyses. Reliability assurance requires the availability of nondestructive evaluation (NDE) techniques not only for defect detection but also for verification of mechanical strength and associated properties. Therefore, NDE should not be defined solely by the current emphasis on the detection of overt flaws. Certainly it is necessary to extend NDE technology to characterize discrete flaws according to their location, size, orientation, and nature. This leads to an improved assessment of the potential criticality of individual flaws. Concurrently, it is necessary to extend NDE techniques for characterizing various material properties. In this case, the emphasis is on evaluation of microstructual and morphological factors that ultimately govern the material's strength and performance. Therefore, a holistic approach which combines nondestructive characterization of defects

with the material environments in which the defects reside is needed. This should lead to improved accuracy in predicting structural integrity and the structure's service life, particularly in the presence of discrete flaws.

This paper reviews the efforts[1-7] expended in evaluating damage characteristics in highly filled polymeric materials under various loading conditions. Several different nondestructive testing techniques, including ultrasonic, acoustic imaging, and real-time radiography, were used to monitor damage initiation and evolution processes. In the subsequent paragraphs, each of these methods will be described and test results will be discussed.

Ultrasonic Techniques

The effects of stain rate and cyclic loading on the cumulative damage in highly filled polymeric materials were determined for two loading conditions, constant strain rate and cyclic strain. The geometry of the specimen used in this study is shown in Fig. 1. Three different strain rates, 0.005 min^{-1}., 0.05 $min.^{-1}$, and 0.5 $min.^{-1}$, were used in the constant strain rate tests. During the cyclic strain test, the strain cycle has a triangular shape and seven strain cycles were applied to the specimen. The minimum strain level for each cycle is 0% and the maximum strain level for the first cycle was 3%. An additional 3% strain level was successively added for each remaining cycle with no rest periods between cycles. After the seventh cycle, the specimens were pulled to failure at a constant strain rate of 0.05 min^{-1}. that was used during the cyclic-strain tests.

During the test, the axial load and transverse displacement was recorded. Ultrasonic measurements were take when sound waves were transmitted through the specimen. A radio-frequency burst of voltage was applied to the acoustic transducer mounted on one face of the specimen. The transmitted signal was received by a second transducer mounted on the opposite face of the specimen. The acoustic measurements were made at a nominal 528 kHz frequency, for which signal-to-noise levels were acceptable. During the tests, a yoke (and level) system was devised to keep the ultrasonic transducers aligned and fixed at the specimen's midpoint during straining. The experimental data were recorded on disk and on the strip chart recorder.

Typical constant strain rate data, plotted as stress vs. strain, are shown in Fig. 2. Typical acoustic data obtained from constant rate tests is shown in Fig. 3. In Fig. 3 the relative changes in the acoustic attenuation coefficient are plotted as functions of the applied axial strain and the strain rate. Note that $\Delta\alpha$ is increased as the applied strain and strain rate are increased. Also note that there is a threshold value of strain, ε_{th}, below which no change in acoustic attenuation occurs. The value of ε_{th} decreases with increasing strain rate. When the strain rate is equal to 0.005 $min.^{-1}$ and 0.05 $min.^{-1}$, ε_{th} is equal to 8% and 4%, respectively. As the strain rate is increased to 0.5 $min.^{-1}$, ε_{th} is equal to zero, and the change in acoustic attenuation was detected as soon as the specimen was stretched. In addition to the strain rate dependency of ε_{th}, the rate of change of $\Delta\alpha$ with respect to strain also increases with increasing strain rate. This is exhibited by the relative steepness of the $\Delta\alpha$ versus ε curve for higher strain rate test data, as shown in Fig. 3. Since $\Delta\alpha$ is proportional to the extent of the internal damage in the material for a given strain level, the increase in $\Delta\alpha$ with increasing strain rate implies that a high strain rate

will induce greater damage in the material. It is interesting to point out that the critical value of the acoustic attenuation coefficient , or the critical damage value, is relatively insensitive to the strain rate.

Typical cyclic stress-strain data is shown in Fig. 4. The data indicate that the cyclic stress-strain curves are different for different strain cycles, and that the difference is increased for each successive strain cycle. The shapes of the loading and unloading branches or the hysteretic loop are similar, and the area within the hysteretic loop or the energy dissipation increases as strain cycles increases. The data also exhibit the typical stress softening known as the "Mullins effect" of strain-induced softening commonly observed in filled polymeric materials such as solid propellants. The degree of strain softening depends of the magnitude of the maximum strain, $(\varepsilon_{max})cy$, of the prior strain cycle. Once the maximum strain of the prior strain cycle is exceeded, the cyclic stress-strain curve has a tendency to join the constant strain rate stress-strain curve as shown in Fig. 4. The figure also shows that a large difference exists between the virgin constant stress-strain curve (Curve A) and the pre-cycled strain rate curve (Curve B) which was obtained by pulling the specimen to fracture immediately after the last strain cycle. Observing Fig. 4, Curve B shows a considerable amount of stress softening when the strain is less than the maximum strain (21%) of the last strain cycle. However, when the strain is higher than 21%, Curve B is above Curve A and a maximum 12% stress increase occurs. This phenomena is highly reproducible and it seems that, for the preloading condition considered in this study, precycling and predamage strengthens the material. This apparent strengthening effect is probably due to: 1) the development of the compressive stress at the end of each strain cycle, 2) the process of material healing, and 3) the change of the microstructures in the material due to precycling.

The acoustic attenuation coefficient, $\Delta\alpha$, is shown as a function of strain under cyclic loading in Fig. 5. Figure 5 reveals that $\Delta\alpha$ exhibits cyclic behavior. The acoustic attenuation during the unloading branch of the cyclic loading is higher than that during the loading branch of cyclic loading. When $(\varepsilon_{max})cy \geq 9\%$, $\Delta\alpha$ continuously increases for the short time period immediately after unloading the specimen from $(\varepsilon_{max})cy$ of the strain cycle, and then it starts to decrease. The magnitude of this initial $\Delta\alpha$ increases as $(\varepsilon_{max})cy$ increases. When $(\varepsilon_{max})cy \leq 6\%$, $\Delta\alpha$ starts to decrease as soon as the specimen starts to unload. However, the magnitude of $\Delta\alpha$ during unloading is higher than that during loading. This kind of cyclic behavior has been observed for other filled polymeric materials. The initial increase in $\Delta\alpha$ immediately after specimen unloading is believed to be related to the local stress and the viscoelastic nature of the material. For a highly filled polymeric material, when the applied stress is decreased, the local stress between particles may still be high enough to cause additional damage and/or to increase the size of the existing voids, resulting in an increase in $\Delta\alpha$. In addition, due to the material's viscoelastic nature, the local time-dependent material response lags behind and is not in phase with the applied deformation[8-9]. The existence of time scale or phase change between the applied load and the local material response is a possible contributing factor responsible for the initial increase during unloading. As the applied load is continuously decreased with time, the local stress will also decrease. When its magnitude is reduced to

a threshold value, no further increase in damage and/or void size can occur. This results in a continuous decrease in $\Delta\alpha$.

In the preceding paragraph, it was mentioned that acoustic attenuation during unloading is higher than during loading regardless of whether there is an initial increase in $\Delta\alpha$ or not. This implies that at a given strain level, the sizes of the voids during unloading are higher than they are during loading. This phenomena is believed to be related to the time-dependent nature of the deformation of the material. In addition, when the specimen is reloaded from 0% strain of the next loading cycle, void sizes are reduced and some healing processes may take place largely due to the compressive stress developed at the end of the prior cycle. Under this condition, it is expected that $\Delta\alpha$ measured during the loading branch of the next strain cycle would be smaller than it was during the unloading branch of the prior strain cycle as shown in Fig. 5.

In the ultrasonic tests, the relative attenuations of acoustic energy were measured under a through-transmission mode. The $\Delta\alpha$ was measured in a small region which is equal to the size of the transducers. Since the microstructure of the uniform is not uniform, the measured $\Delta\alpha$ may depend on the location of the transducers attached to the specimen's surfaces. To measure the damage state along the gauge length of the specimen, two ultrasonic transducers were centrally mounted 0.5 in. (1.27 cm) apart along the gauge length of the specimen. In this study, fracture and cyclic loading tests were conducted under a constant strain rate of 2.2 $min.^{-1}$ at room temperature. For the fracture test the specimen was stretched until the specimen was fractured. For the cyclic loading test, the specimen was loaded to 12% strain and then unloaded to 0% strain. The acoustic measurements were made at a 8 Mhz frequency.

Figure 6 shows the energy content decreases during the specimen's life. The initial rapid decrease in energy content may be due to the absorption and scattering effects of the dewetting and vacuole formation processes. Smaller energy-content differences between consecutive measurements are observed during the latter portion of the specimen's lifetime when vacuole growth and coalition and macroscopic crack formation are believed to dominate.

Figure 7 shows the result of a loading-unloading test. According to Fig. 7, the energy content decreases with increasing stress during the loading cycle and the energy content continuously decreased in a short time period immediately after the specimen was unloaded. The phenomenon is consistent with that observed in the ultrasonic attenuation measurement under cyclic loading condition discussed earlier.

Acoustic Imaging Technique

In this study the Lockheed-Martin Research Laboratory's acoustic-imaging system was used to measure the attenuation difference in a scanning mode. During the test the acoustic wave of a wavelength short enough to exhibit quasioptical behavior was radiated from an insonifier combined with a plan concave polystyrene lens, which focused acoustic energy at a desired location in the material to be studied. Acoustic energy passing through the material was recovered by a receiver lens similar of similar geometry and configuration, which transmitted the acoustic energy to a receiving transducer. The

receiving transducer converted acoustic energy into a corresponding electrical signal which was stored in a computer for further data analysis.

A two-dimensional acoustic image was generated in a common focal plane of the lenses by mechanical translation of the two lens/transducer units together in a plane normal to the acoustic transmission path. Each translation generated one scan line in the image. After each scan line had been completed, the scan mechanism stepped one unit in elevation, and another line scan was performed. Approximately 512 data points were generated per scan line, and 100 lines were scanned per inch of test material. An ultrasonic frequency of 1.9 Mhz was used in the test.

The recorded experimental data were processed to create a visual indication of the energy absorbed in the material being inspected. A region of high ultrasonic absorption, i.e., a highly damaged area, will be shown as a dark area and a region of unattenuated ultrasonic wave will produce a light or white area with 255 shades of gray in between. The acoustic image at a given strain level was plotted in the form of isointensity contours of the transmitted acoustic energy, I_t, to enhance the resolution of the damage field. The results of these analyses are discussed in the following paragraphs.

Plots of isointensity contours of I_t as a function of the applied strain are shown in Fig. 8. In Fig. 8 the number between two contour lines is the range of I_t between the prior and the next intensity level. The small number indicates that the intensity of the transmitted acoustic energy is low, or the damage level is high. It should be mentioned that because of acoustic diffraction, the size of the apparent crack as shown in Fig. 8 is relatively larger than the actual crack. Referring back to Figs. 8a and 8b. it is seen that the size of the damage zone and the severity of the damage in the damage zone increase as the strain level increases. The phenomenon, under a monotonically increasing load condition, is expected because as the strain level increases, the severity of the damage and the damage zone size increase. When the specimen is unloaded from 6% to 3% strain, a comparison of Figs. 8a and 8c reveals that the damage zone size and degree of damage at 3% strain during unloading are greater than they are at 3% strain during loading. This indicates that a large amount of damage can develop near the crack tip region when the strain is increased from 3% to 6% strain during the loading branch of the strain cycle. It is interesting to note that, when the applied strain is reduced from 6% to 3%, the size of the highly damaged region, $I_t = 10$, is increased.

At the end of each strain cycle, because large deformation occurs near the crack tip, the deformed material doesn't return to its original strain-free condition even though the applied strain is 0%. Thus, a compressive residual stress and tensile residual strain region is developed near the crack tip. The existence of the tensile residual strain near the crack tip will prevent the microcracks and microvoids, generated by previously applied strain, from closing in spite of the existence of the compressive residual stress field. In addition, due to the material's viscoelastic nature, a time scale or phase shift exists between the applied load and the microscopic (local) deformation of the material. Thus, some time is required to rearrange the microstructure, such as the movement of filler particles within the material, to respond to the load. These may be the reasons why the damage zones still exist when the specimen is unloaded to 0% strain. However, as time elapses, microvoid size will decrease due to the time-dependent nature of the material deformation process. The decrease in microvoid size with increasing time should be manifested by the increase

in I_t value. In other words, damage zone size and damage intensity decrease as the length of time is increased. This time-dependence of damage characteristics, measured by the acoustic imaging technique, is clearly indicated in Fig. 9.

In the previous paragraph we discussed the damage characteristics near the crack tip determined using the acoustic imaging technique. Since it takes time to scan the specimen, the acoustic imaging technique is a good technique to measure damage characteristics near the tip of a stationary crack. In order to measure the damage characteristics near the tip of a propagating crack, Lockheed-Martin's High-Energy Real-Time (HERT) Imaging System was used and the results of the studies are discussed in the following paragraph.

Figure 10 shows the contours of transmitted x-ray energy near the tip of a propagating crack under a constant strain rate condition. In this figure, the number between two contour lines is the minimum intensity level of a range of I_t between the minimum intensity level and the next intensity level. A small number indicates that the intensity of the transmitted x-ray energy is low or that the damage is high. These contour plots show the details of the size and shape of the damage zone as well as the damage intensity inside the damage zone. It is interesting to note that not only the damage zone size but also the damage zone shape changes before and during crack propagation.

Figure 11 shows the damage characteristics near the tip of the propagating when the specimen was held at a constant strain. From Fig. 11 we see that the crack tip is blunted and damage intensities in and near the two small damage zones are increased. As time elapses, a large void is generated above the crack tip as indicated in Fig. 11. Finally, the main crack tip and the void are joined, leading to the fracture of the specimen.

CONCLUSIONS

In past years, a considerable amount of effort was spent in obtaining a fundamental understanding of damage initiation and its evolutionary process as well as the effects of damage on the material's constitutive and crack growth behavior in highly filled polymeric materials. Much of what we know about the damage process under different loading conditions has been obtained using nondestructive testing techniques. During the course of the damage studies, different nondestructive testing techniques were used. The advantages and disadvantages of each technique were discussed. Due to the viscoelastic nature of the materials, load history and time have a significant impact on the damage characteristics in the materials. Therefore, caution should be exercised when interpreting the nondestructive testing results.

REFERENCES:

(1) Liu, C. T.," Effect of Load History on the Cumulative Damage in a Composite Solid Propellant" AIAA paper No. 86-1015.

(2) Liu, C.T. and Tang, B." Investigating Cumulative Damage in a Highly Filled Polymeric Material," Mechanics of Materials and Structures Studies in Applied Mechanics, Vol.35, Feb. 94, Elsevier Science.

(3) Tang, B., Liu, C. T.,and Henneke, E. G.," Acoustic-Ultrasonic Technique Applied to the Assessment of Damage in a Particulate Composite," Journal of Spacecraft and Rockets, Vol.32, No.5,1995.

(4) Liu, C. T.,"Evaluation of Cumulative Damage in a Composite Solid Propellant" Society of Experimental Mechanics 1986 Spring Conf. June, 1986.

(5) Liu, C. T." Investigating the Damage Field Near the Crack Tip in a Composite Solid Propellant," Society of Experimental Mechanics 1987 Spring Conf., June1987.

(6) Liu, C. T.," On the Evaluation of Damage Fields Near Crack Tips in a Composite Solid Propellant," Journal of Spacecraft and Rockets, Vol.28, No.1, 1991.

(7) Liu, C.T. and Tang, B.," Investigating Damage Fields in a Particulate Composite Material Using the Real-Time X-Ray Technique," SPIE's 1993 International Symposium on Optics, Imaging, and Instrumentation, San Diego, CA, July 11-16,1993

(8) William, M. L., "Fatigue-Fracture Growth in Linear Viscoelastic Material" Journal of Physics, 38 (11) Oct. 1967.

(9) Knauss, W. G., and Dietmann, H., " Crack Propagation Under Variable Load Histories in Linearly Viscoelastic Solids," Int. J. Engrg. Sci., Vol.8, 1970.

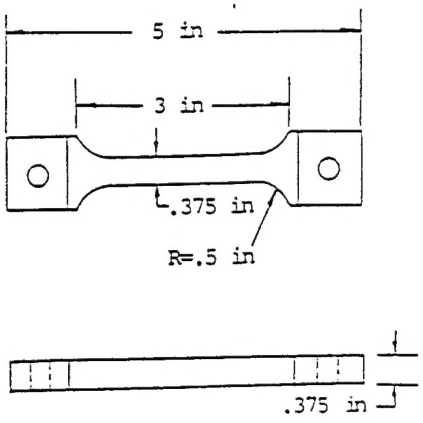

Fig.1 Specimen geometry

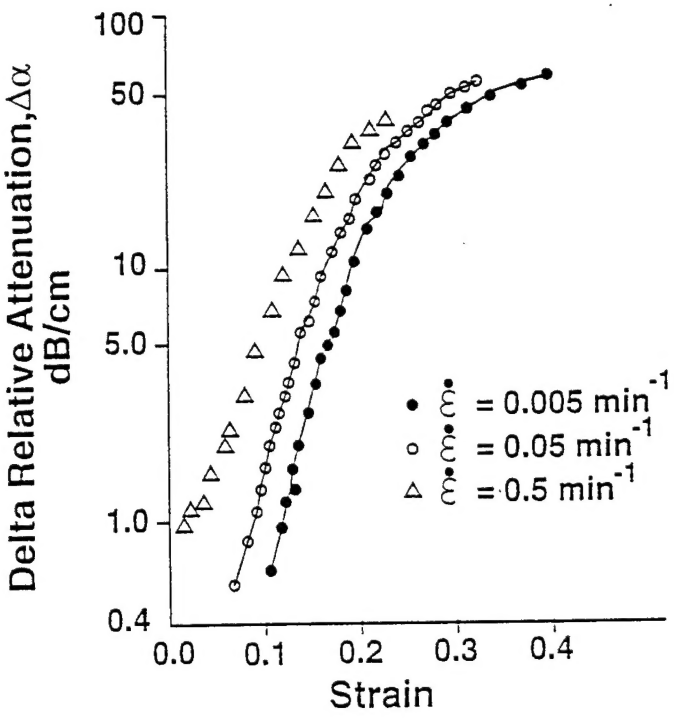

Fig.3 Relative change in acoustic attenuation versus strain (constant strain rate loading)

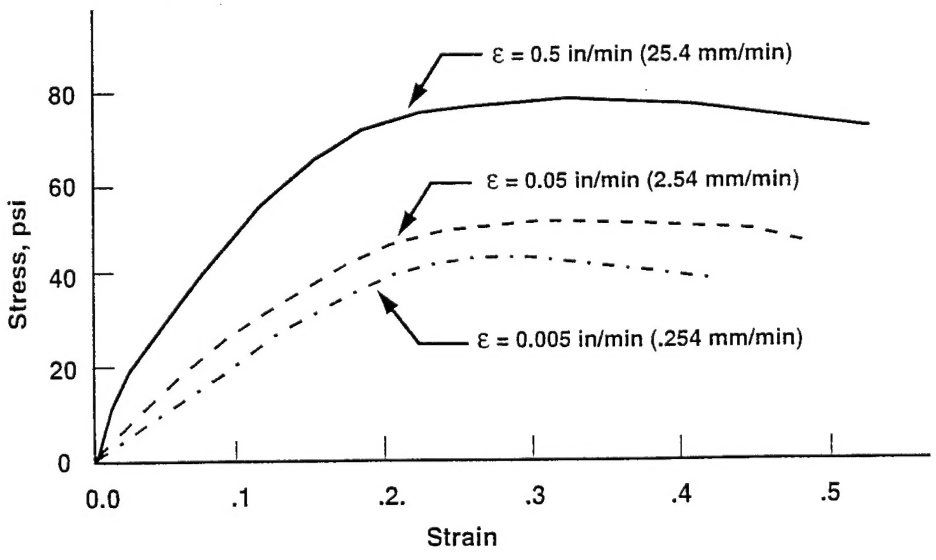

Fig.2 Stress-strain curves as functions of strain rate.

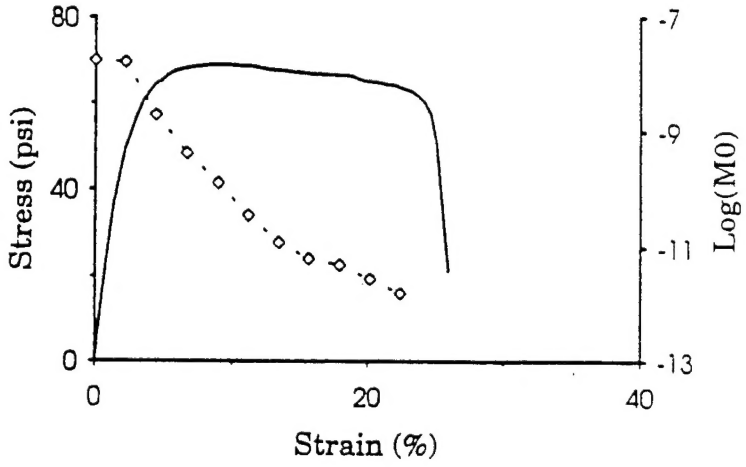

Fig. 6 Plot of stress and ultrasonic energy (Mo) as functions of strain (constant strain rate loading)

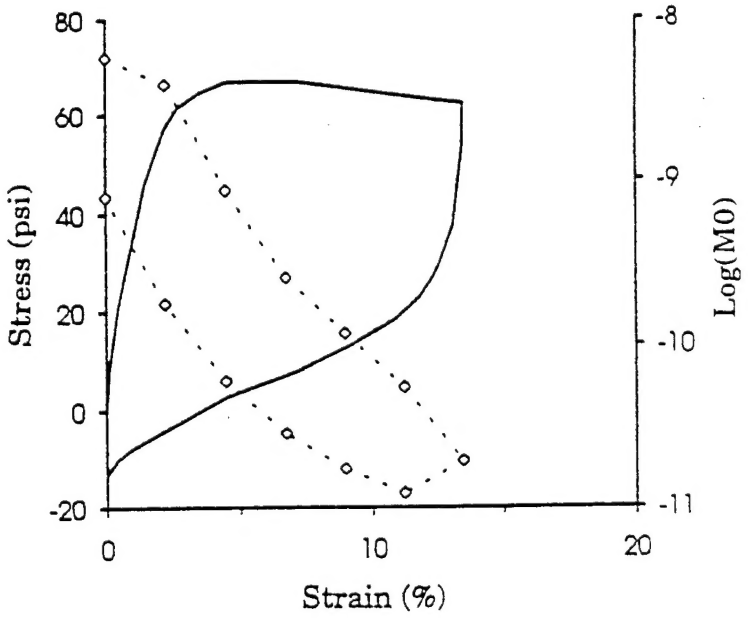

Fig. 7 Plot of stress and ultrasonic energy (Mo) as functions of strain (cyclic loading)

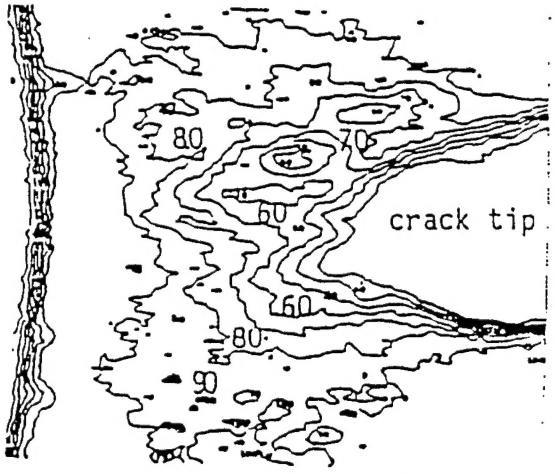

ϵ = 13.5%

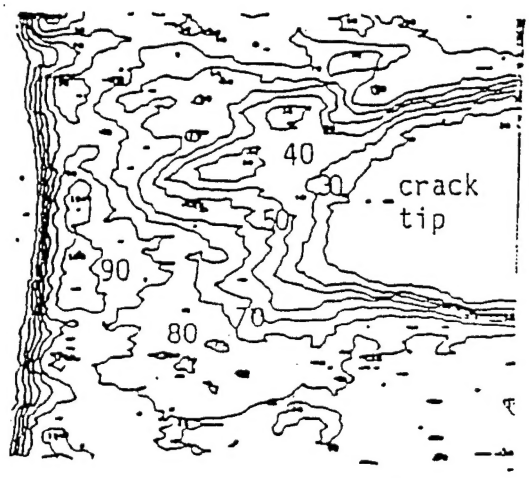

ϵ = 13.5%

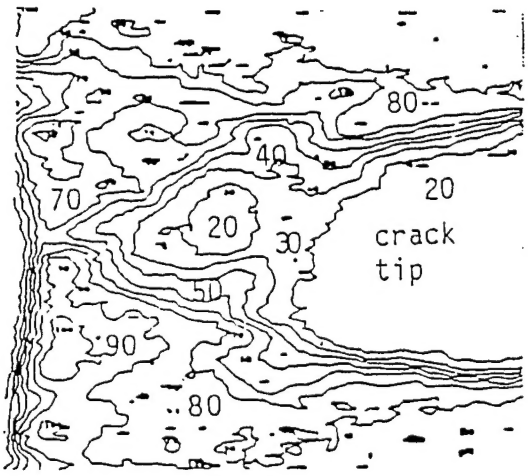

ϵ =13.5%

Fig.11 Iso-intensity contour plots of the x-ray energy transmitted through the specimen at 13.5% constant applied strain.

PAGES FIGS. 4,5,8,9,10 ARE MISSING IN ORIGINAL DOCUMENT